LANGMUIR Article
Cite This: Langmuir 2018, 34, 425−431
pubs.acs.org/Langmuir

Polyelectrolyte Capping As Straightforward Approach toward Manipulation of Diffusive Transport in MOF Films

Juan A. Allegretto,[†,‡] Jimena S. Tuninetti,[†] Agustín Lorenzo,[†] Marcelo Ceolín,[†] Omar Azzaroni,[†] and Matías Rafti*[,†]

[†]Instituto de Investigaciones Fisicoquímicas Teóricas y Aplicadas (INIFTA), Departamento de Química, Facultad de Ciencias Exactas, Universidad Nacional de La Plata, CONICET, Calle 64 y Diag. 113, 1900 La Plata, Argentina

[‡]Universidad Nacional de San Martín (UNSAM), San Martín, Argentina

Supporting Information

ABSTRACT: We present experimental results demonstrating the suitability of polyelectrolyte capping as a simple and straightforward procedure to modify hydrophilic/hydrophobic character of porous films, thus allowing additional control on transport properties. In particular, we synthesized ZIF-8 metal organic framework (MOF) films, an archetypal hydrophobic zeolitic imidazolate framework, constituted by Zn^{2+} ions tetrahedrally coordinated with bidentate 2-methylimidazolate organic linker, and poly(4-styrenesulfonic acid) as capping agent (PSS). MOF films were synthesized via sequential one pot (SOP) steps over conductive substrates conveniently modified with primer agents known to enhance heterogeneous nucleation, followed by dip-coating with PSS aqueous solutions. Crystallinity, morphology, and chemical composition of ZIF-8 films were confirmed with traditional methods. Continuous electron density depth profile obtained with synchrotron light X-ray reflectivity (XRR) technique, suggest that PSS capped-films do not adopt segregated configurations in which PSS remains surface-confined. This affects functional properties conferred by PSS capping, which were assessed using cyclic voltammetry with both positively and negatively charged redox probe molecules. Furthermore, taking advantage of the control attained, we successfully carried in situ synthesis of film-hosted d-block metal nanoparticles (Au and Pt-NPT@5*x*-ZIF-8+PSS) via direct aqueous chemical reduction of precursors (diffusion-reaction approach).

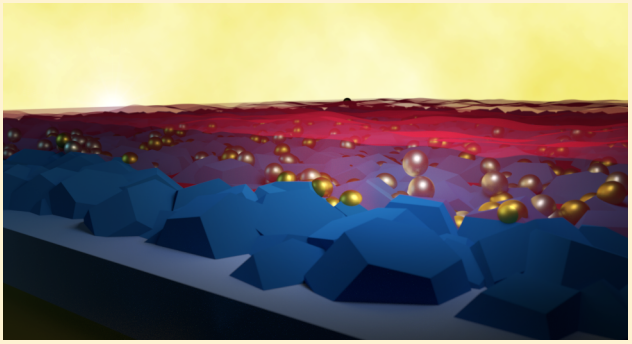

INTRODUCTION

Engineering functional porous materials at the nanometer scale requires a detailed control on fundamental interactions between its building blocks. If the goal is to obtain a predefined porous structure with selected chemical moieties exposed, then a suitable strategy would be to employ, for example, postsynthetic modification. Metal organic frameworks (MOFs), featuring metal-containing units coordinated with organic multidentate linkers, constitute an emergent and relatively new class of permanently porous solid material, which fits the above description.[1,2] Appealing examples in which MOFs structural and chemical flexibility find application are its uses as porous supports, e.g., in the fabrication of microdevices (via enzyme immobilization through the so-called "nanoarchitectonics" approach, as coined by Ariga et. al),[3−6] or various sensor-related applications, energy conversion devices, catalysis, and both, gas and liquid phase separation technologies.[7−12] Because many of these applications involve MOF films, a considerable amount of effort has been devoted to study different growth and anchoring strategies, and to explore suitable characterization techniques.[13−19] A crucial property to look at when, for example, synthesizing MOF films over conductive substrates for electrochemical applications, is molecular transport through such porous interfaces.[20−23] Manipulation of molecular permeances can be carried via inclusion of a selected capping agent to the film architecture which would provide such feature. If polyelectrolytes are used for capping, then a variation on polar character can be expected; such a strategy has been proved to be adequate for mesoporous silica thin films modification,[24] which in turn allowed researchers to obtain well-dispersed metal nanoparticles hosted at the mesoporous support,[25] an active composite heterogeneous catalyst for gas-phase low-pressure ammonia oxidation.[26]

An interesting MOF subclass is the so-called zeolitic imidazolate frameworks (ZIFs), featuring divalent metal cations tetrahedrally coordinated by bidentate imidazolate-derived organic linkers; its name refers to a zeolite-like topology related to the similarity between N−metal−N and O−Si−O bond angles. Solvothermal methods for ZIFs

Received: August 31, 2017
Revised: December 6, 2017
Published: December 11, 2017

DOI: 10.1021/acs.langmuir.7b03083
Langmuir 2018, 34, 425−431

synthesis are straightforward and robust, and the obtained materials have relatively high chemical and physical stabilities among MOFs.[27,28] Because of their intrinsic microporosity and large surface areas, ZIFs prompted an intense research activity devoted to explore possible applications in gas and liquid phase adsorption, separations, and heterogeneous catalysis.[29−32] ZIF-8 (available commercially as BASF-BASOLITE-Z1200) is an archetypal member of this subclass constituted by Zn^{2+} metal ions tetrahedrally coordinated by 2-methylimidazolate (2-mIm) bidentate linkers, featuring ∼11.6 Å diameter cages with ∼3.4 Å pore windows, and a nominal BET surface area of ∼1800 m^2/g. We have recently studied ZIF-8 films synthesis via sequential one-pot (SOP) steps over conductive substrates with an in situ Quartz Crystal Microbalance (QCM) setup.[33] Inspired by the reported synthesis of stable polymer@MOF composite materials using Poly(4-styrenesulfonic acid) (PSS) and ZIF-8 (taking advantage of the affinity between sulfonate moieties and Zn^{2+} metal ions),[34] it was also shown recently the suitability of this approach for film formation. Surface modification using $-SO_3H$-terminated self-assembled monolayers (SAMs) or even polymer brushes, were shown to be effective for anchoring and promoting rapid growth of ZIF-8 films.[35] Using this primers allowed to explore and tune interesting properties such as hierarchical micro- and mesoporosity, evidenced by the observed thickness-dependent diffusion of redox probes.[36] Moreover, by improving the ability to grow robust films, a number of possible applications emerged, such as, for example, an enhancement effect on the electrochemical oxygen reduction reaction (ORR) when carried on composite ZIF-8/conducting polymers electrode.[37]

Having in mind the above-discussed ideas, ZIF-8 films were synthesized over conductive substrates modified with suitable primers, via sequential one pot procedure (SOP). Crystallinity, morphology, and chemical composition were characterized using ATR-FTIR spectroscopy, surface zeta potential, X-ray diffraction, wide-angle X-ray scattering (WAXS), contact angle goniometry, and scanning electron microscopy. To explore molecular permeation of both negatively and positively charged redox probes through these polyelectrolyte-modified porous films, we conducted cyclic voltammetry experiments. Results obtained points toward a decrease on the ZIF-8 film's hydrophobic character caused by PSS capping, which demonstrate the suitability of the hereby proposed permeation control strategy. Additionally, and quite different from previously reported strategies,[38] we have taken advantage of the above-mentioned increased polarity and performed aqueous in situ synthesis of film-hosted Au and Pt nanoparticles (Au-NPT@*5x*-ZIF-8+PSS and Pt-NPT@*5x*-ZIF-8+PSS) via direct chemical reduction of diffusively preloaded precursors.[39] UV−visible spectra confirmed the presence of characteristic Au-NPT plasmon only for PSS-capped films; furthermore, we present results of both X-ray Photoelectron Spectroscopy (XPS), and synchrotron-light based X-ray reflection (XRR) experiments showing that lateral NPT distribution for PSS-capped films can be considered as continuous (i.e., ruling out configurations in which NPT remain surface-confined).

EXPERIMENTAL SECTION

Materials Used, Synthesis, and Procedures. All reagents were used as supplied by Sigma-Aldrich, zinc nitrate hexahydrate, 2-methylimidazole (HmIm), 3-triethoxysilylpropylamine (APTES), Hydrogen tetrachloroaurate(III) hydrate, hydrogen hexachloroplatinate(IV), sodium borohydride, hexaammineruthenium(II) chloride, hexaammineruthenium(III) chloride, potassium chloride, potassium hexacyanoferrate(II) trihydrate, potassium hexacyanoferrate(III), sodium 3-mercapto-1-propenesulfonate (MPSA), methanol, ethanol, PSS and toluene. The solutions were prepared with milli-Q water or methanol.

Because of the variety of experimental techniques used for characterization, substrates with distinctive properties were needed in each case; e.g. for XRR, low roughness is of paramount importance, thus APTES modified monocrystalline Si wafers (featuring NH_2 moieties that act as nucleation sites for heterogeneous film growth) were used. For electrochemical experiments, conductive substrates were needed, then either polycrystalline Au surfaces (modified with MPSA self assembled monolayers) or APTES-modified indium tin oxide (ITO) substrates were employed. For Au-NPT@*5x*-ZIF-8+PSS films characterization, substrates transparent to radiation were needed; therefore, APTES-modified quartz glass substrates were used.

Modification of Substrates. For surface modification of the substrates, procedures elsewhere reported were applied.[36] Briefly, ITO substrates, Si monocrystalline wafers, and quartz substrates, were subjected to a cleaning protocol consisting in sequential application of soapy water, deionized (DI) water, acetone, and ethanol in an ultrasonic bath for 10 min each, followed of nitrogen drying. The chemical surface functionalization was carried via treatment of clean glass, ITO, and Si substrates with APTES solution (0.2 mM in Toluene) at 90 °C overnight, followed of extensive ethanol washing and nitrogen drying. For the Au substrates, the surface modification was carried using MPSA (20 mM in 10 mM sulfuric acid aqueous solution). The Au substrates were first washed using the above-described procedure for ITO, and then exposed to MPSA solution overnight followed by DI water washing and nitrogen drying.

ZIF-8 Film Synthesis. Synthesis of ZIF-8 films was carried via room temperature direct mixture of methanolic $Zn(NO_3)_2$ (25 mM) and HmIm (50 mM) solutions in plastic vials where the substrate was face-down immersed for 30 min, followed by methanol rinsing and nitrogen drying. This whole sequence constitutes one growth cycle; when *n* of such cycles were performed, the obtained films are referred as *nx*-ZIF-8. To ensure suitable thickness for an exploration of polyelectrolyte capping effect $n = 5$ growth cycles were used.

PSS Capping. For the polyelectrolyte capping procedure, 1 mg/mL aqueous PSS solutions ($M_w \approx 70$ kDa) where prepared. The *5x*-ZIF-8 films were contacted with these solutions for 20 min and then, rinsed with DI water and dried as above-described. These films will be referred hereafter as *5x*-ZIF-8+PSS.

Au- and Pt-NPT@5x-ZIF-8+PSS Films. A straightforward procedure for Au and Pt nanoparticles synthesis was followed. As earlier reported,[25] solutions of NPT precursors were sequentially contacted with MOF films synthesized over transparent substrates. After overnight soaking in 1 mM milli-Q water solution of NPT precursors in order to ensure diffusion into the mesoporous films, and then thoroughly rinsed with milli-Q water followed by nitrogen drying. The reduction was carried by immersing the substrates in $NaBH_4$ solutions; the extent of Au-NPT formation was followed as a function of the immersion time using UV−vis absorption of nanoparticle plasmon, while lateral distribution was determined with Ar-ion sputtering and XPS experiments. Pt-NPT lateral distribution was explored using synchrotron light XRR experiments. Schematic representation of the complete procedure followed in order to obtain the above-described films is illustrated in Scheme 1.

Characterization Techniques. *Surface Zeta Potential.* Surface zeta potential measurement was performed at 25 °C in a Malvern's Zetasizer Nano ZS.

XRR. X-ray Reflectometry (XRR) experiments were performed at the D10AXRD2 beamline of Laboratorio Nacional de Luz Sincrotron (LNLS) (Campinas, Brazil) ($\lambda = 1.608$ Å). The sample-to-detector distance was kept to 550 mm, the scattered beam was detected using a PILATUS 100 K detector (DECTRIS AG, Switzerland).

WAXS. Crystalline structure of films was confirmed using wide-angle X-ray scattering (WAXS). The SAXS/WAXS system (INIFTA, project "Nanopymes", EuropeAid/132184/D/SUP/AR-Contract

DOI: 10.1021/acs.langmuir.7b03083
Langmuir 2018, 34, 425−431

Scheme 1. Illustration of the Procedure Followed in Order to Synthesize Metal Nanoparticles@porous Films

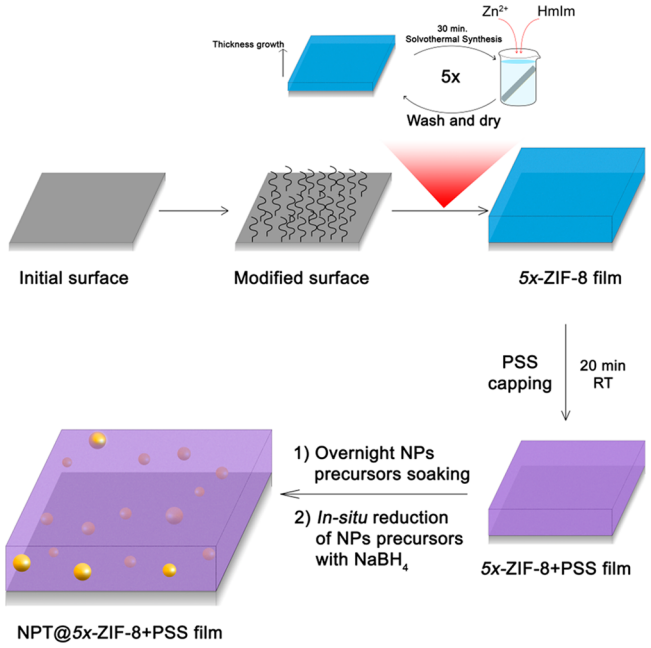

331−896) is a XEUSS 1.0 HR (XENOCS, Grenoble) equipped with a microfocus X-ray source and a Pilatus 100 K detector (DECTRIS AG, Switzerland).

ATR-FTIR. Vibrational spectra were obtained in order to characterize chemical composition after and before polyelectrolyte capping. Measurements were carried with a FTIR-Varian 660 infrared spectrometer using single-point ATR configuration with a ZnSe crystal.

Cyclic Voltammetry. Cyclic-voltammetry (CV) experiments were carried with a three-electrode cell configuration; films as the working electrode, whereas saturated Ag/AgCl and Pt were used as reference and counter electrode, respectively. Positively and negatively charged redox probes used were $Fe(CN)_6^{4-/3-}$ and $Ru(NH_3)_6^{2+/3+}$ prepared using 1 mM concentration in each case, and 0.1 M KCl solution with milli-Q water. A Gamry-instruments Reference 600 potentiostat was used in all experiments.

Contact Angle. The water-contact angle of the films 5*x*-ZIF-8 and 5*x*-ZIF-8+PSS were measured with a Ramé-Hart System model 290 in a static-drop configuration.

UV−Vis Spectroscopy. Ocean Optics USB4000 spectrometer was used for absorption spectra measurements.

SEM. Scanning electron microscopy technique was used in order to characterize morphologies obtained, images were taken using both ESEM (FEI Quanta 200-LIMF) and FE-SEM (model SUPRA40 Carl Zeiss) apparatus.

XPS. Chemical film composition in different depths was determined using X-ray photoelectron spectroscopy (XPS). Argon ion sputtering was used in order to expose different depths of synthesized films with SPECS Sage HR 100 spectrometer equipped with nonmonochromatic X-ray source (Aluminum Kα line of 1486.6 eV energy and 300 W). Also, PSS presence was double checked by identification of S 2s characteristic XPS signal.

RESULTS AND DISCUSSION

ATR-FTIR. ATR-FTIR experiments carried on films synthesized are presented in Figure 1, which shows an enlarged section of the whole wavenumber range explored, corresponding to the stretching-zone where signature PSS vibrational bands appear only on for ZIF-8+PSS modified films. Peaks at 830 and 1040 cm^{-1} wavenumber, corresponding

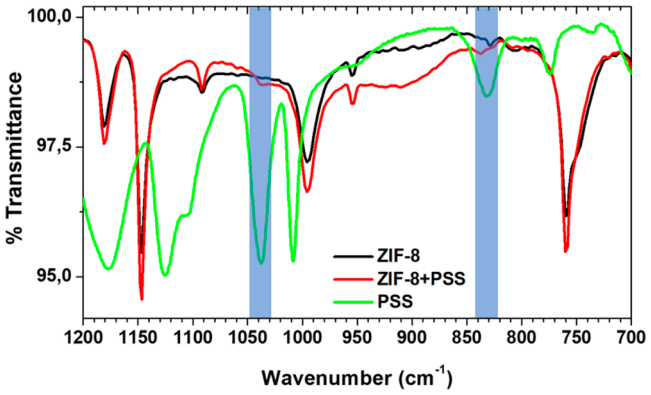

Figure 1. Vibrational spectra of 5*x*-ZIF-8, 5*x*-ZIF-8+PSS, and PSS. Peaks at 830 and 1040 cm^{-1} wavenumber, corresponding respectively to S−O and S═O stretching modes can be observed. The characteristic PSS bands at 1038 and 1008 cm^{-1} are present, but because of the background can only be distinguished as small peaks superimposed to ZIF-8 signature peaks.

respectively to S−O and S═O stretching modes can be observed. Complete spectra of ZIF-8 and PSS can be found in the Supporting Information file.

Contact Angle. Film contact angle was measured in order to illustrate the effect of PSS modifications. Figure 2 shows the

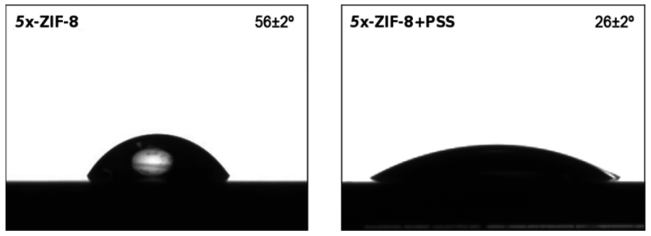

Figure 2. Contact angle of 5*x*-ZIF-8 film (left, 56±2°), and its change after PSS modification (right, 26±2°).

change observed when 5*x*-ZIF-8 films were capped with PSS. Wettability of the surface can be understood in terms of an increase in surface polar character induced by sulfonate moieties exposed after capping.

Crystalline Structure. WAXS experiments were conducted in order to obtain information on the crystal structure of the ZIF-8 films obtained. Figure 3 show the correspondence of calculated diffractograms with those obtained for the film before and after capping, thus confirming that crystalline structure remains unperturbed (aside from some small relative intensity differences, which are to be expected due to the effect of a modifying agent of film surface, such as PSS). Film morphology is not altered by PSS capping, which is shown in the Supporting Information file SEM images and complementary XPS experiments.

Surface Zeta Potential. To understand permeation properties of synthesized films, Surface Zeta Potential for 5*x*-ZIF-8 was measured. The value obtained is slightly negative (−13 ± 1 mV), experimental details are given in the Supporting Information.

Cyclic-Voltammetry Experiments. Charged redox probes (both positive and negative, $Ru(NH)_6^{3+/2+}$ and $Fe(CN)_6^{3-/4-}$, respectively) were used for CV experiments performed using as working electrodes 5*x*-ZIF-8 and 5*x*-ZIF-8+PSS films grown over conductive polycrystalline Au

DOI: 10.1021/acs.langmuir.7b03083
Langmuir 2018, 34, 425−431

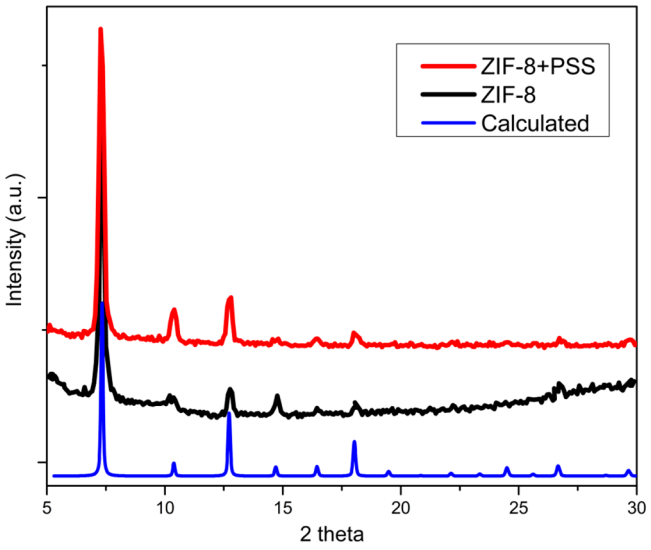

Figure 3. *5x*-ZIF-8 film and PSS capped film compared with calculated diffractogram. Main diffraction peaks present on synthesized samples can be identified as 2θ value increases: (110), (200), (211), and (220), for 2θ = 15.

substrates. Experiments aimed to elucidate the effect of PSS-capping on film transport properties, since redox probes used have similar hydrodynamic diameters (~6 Å), diffusion should only occur through the available intergrain mesoporosity, given that ZIF-8 pore window size (~3 Å) is not big enough to allow intragrain microporosity to be involved in such process. Figure 4 shows the results obtained for all the configurations and

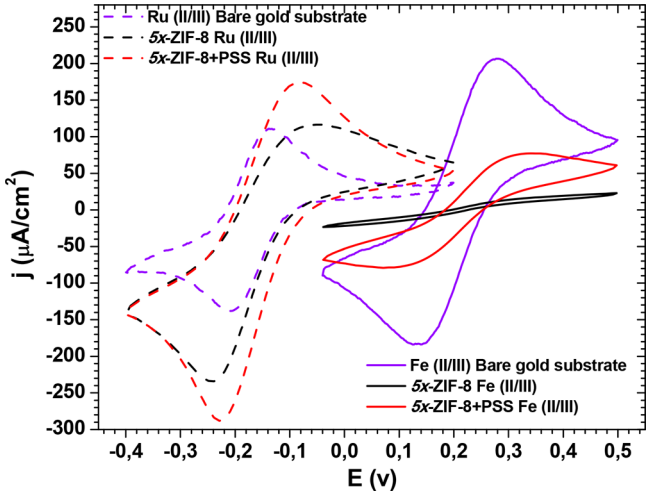

Figure 4. Current density vs potential response of *5x*-ZIF-8 and *5x*-ZIF-8+PSS films for $Fe(CN)_6^{4-/3-}$ (right), and $Ru(NH_3)^{2+/3+}$ (left) in 0.1 M KCl at 25 mV/s.

redox probe tested. Looking closely to $Fe(CN)_6^{3-/4-}$ voltammograms (Figure 4, right), a clear charge-exclusion effect is present when comparing bare Au and *5x*-ZIF-8, which could be traced back to slightly negative film's Z-potential as already discussed (see above, and Supporting Information file). Further support to this interpretation is given by $Ru(NH)_6^{3+/2+}$ voltammograms presented in Figure 4 (left), for which an increased peak current density for ZIF-8 film compared to the bare Au substrate surface is observed instead. If we now compare $Ru(NH)_6^{3+/2+}$ and $Fe(CN)_6^{3-/4-}$ voltammograms for PSS capped films (*5x*-ZIF-8+PSS), an increased electrochemical signal can be observed in both cases (quantitative comparison taken from integrated areas of CV experiments can be founded in Supporting Information file). In order to understand such behavior, it is necessary to take into account two effects which operate in a concurrent way, (i) charge exclusion due to ZIF-8 film Z-potential, and (ii) an increased wettability provoked by PSS capping. Charge exclusion effect would explain the difference between bare Au substrates and ZIF-8 films ($Fe(CN)_6^{3-/4-}$ decreased permeation vs $Ru(NH)_6^{3+/2+}$ increased permeation. After PSS capping, the permeation channels gain an increased polar character, which would explain the relatively high current density obtained for both probe molecules tested. In other words, PSS causes a decoupling of charge exclusion effect observed for negative redox probes. It should also be pointed out that peak current density for $Ru(NH)_6^{3+/2+}$ in both *5x*-ZIF-8 and *5x*-ZIF-8+PSS films is higher than its value for the bare Au substrate. This can be understood in terms of a preconcentration effect on the film operating only for the positively charged redox probe.

UV−Vis Experiments for Au-NPT Synthesis over ZIF-8 Films and ZIF-8+PSS Films. Taking advantage of the above-described gained control on polar character of film's mesoporosity, we explored its suitability as support for the aqueous synthesis of composite materials with homogeneously distributed embedded gold nanoparticles (Au-NPT). The confined formation of Au-NPT carried as described above, was followed in situ through UV−vis Spectroscopy. The absorbance plots presented in Figure 5 recorded in transmission configuration show the appearance of characteristic Au-NPT plasmon after consecutive $NaBH_4$ reduction cycles of 5 and 10 s with reducing agent, only for the PSS capped films. This result is in line with the observed exclusion effect, highly relevant for negatively charged molecules (chlorine coordinated D-metal complexes) normally used as nanoparticle precursors.

XPS Depth-Profiles for Au-NPT Synthesized over Both *5x*-ZIF-8 and *5x*-ZIF-8+PSS Films. Argon ion sputtering experiments were carried in order to determine chemical composition depth-profiles, which would bring further insight on film configurations obtained. Figure 6 show the Zn-2p, N-1s and Au-4f signals obtained from Au-NPT@*5x*-ZIF-8+PSS film at different sputtering times, which translates into different depths. As can be concluded from the plots, Au NPT are present on the film within the penetration depth probed with XPS before sputtering. For increasingly higher sputtering times, a strong signal corresponding to Au^0 at 84 eV binding energy appears, which suggest the presence of Au-NPT within the PSS-capped films. For long sputtering times, Au binding energies founded become slightly shifted to higher values than the expected for Au^0, this could be rationalized by taking into account a remaining nonreduced Au-precursor population near the substrate region of the film after the 10 s exposure to reducing agent.

X-ray Reflectivity (XRR) Experiments with Synchrotron Light for Pt-NPT@*5x*-ZIF-8+PSS Films. To show the versatility of the hereby proposed approach to film control, high electron density Pt nanoparticles were also synthesized following identical procedure as described above for Au-NPT. XRR results are presented in Figure 7, curves obtained for bare, PSS-capped, and Pt-NPT@*5x*-ZIF-8+PSS films are presented. Bare ZIF-8 films present a very well-defined peak at 0.52 $Å^{-1}$, and two smaller peaks at 0.73 and 0.90 $Å^{-1}$; relative peak

DOI: 10.1021/acs.langmuir.7b03083
Langmuir 2018, 34, 425−431

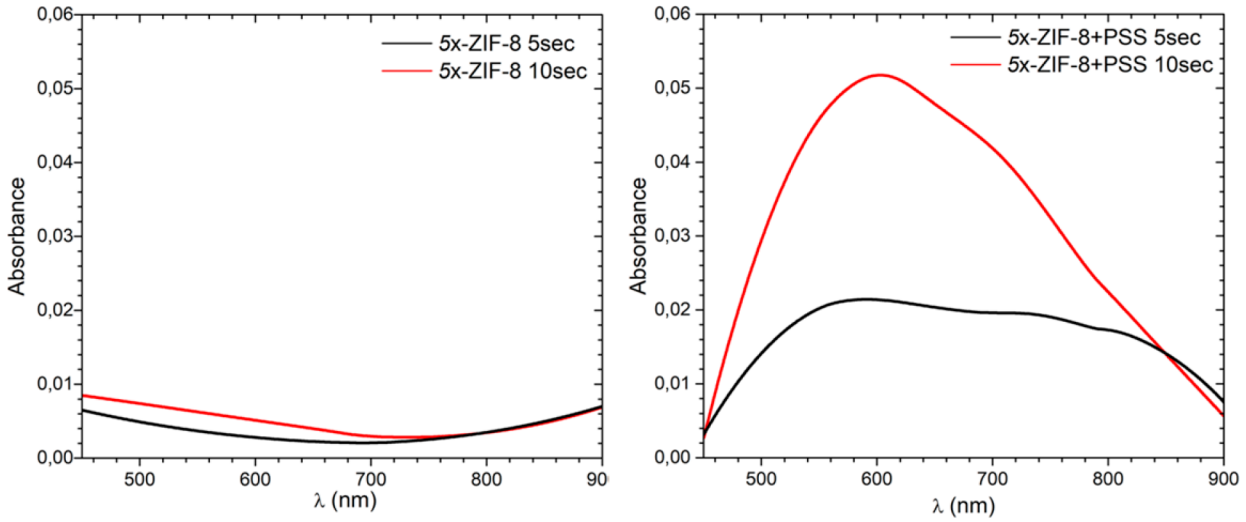

Figure 5. UV−vis absorption experiments for in situ Au-NPT formation triggered by exposure to $NaBH_4$ reducing agent on both, noncapped *5x*-ZIF-8 (left), and *5x*-ZIF-8+PSS (right) capped films.

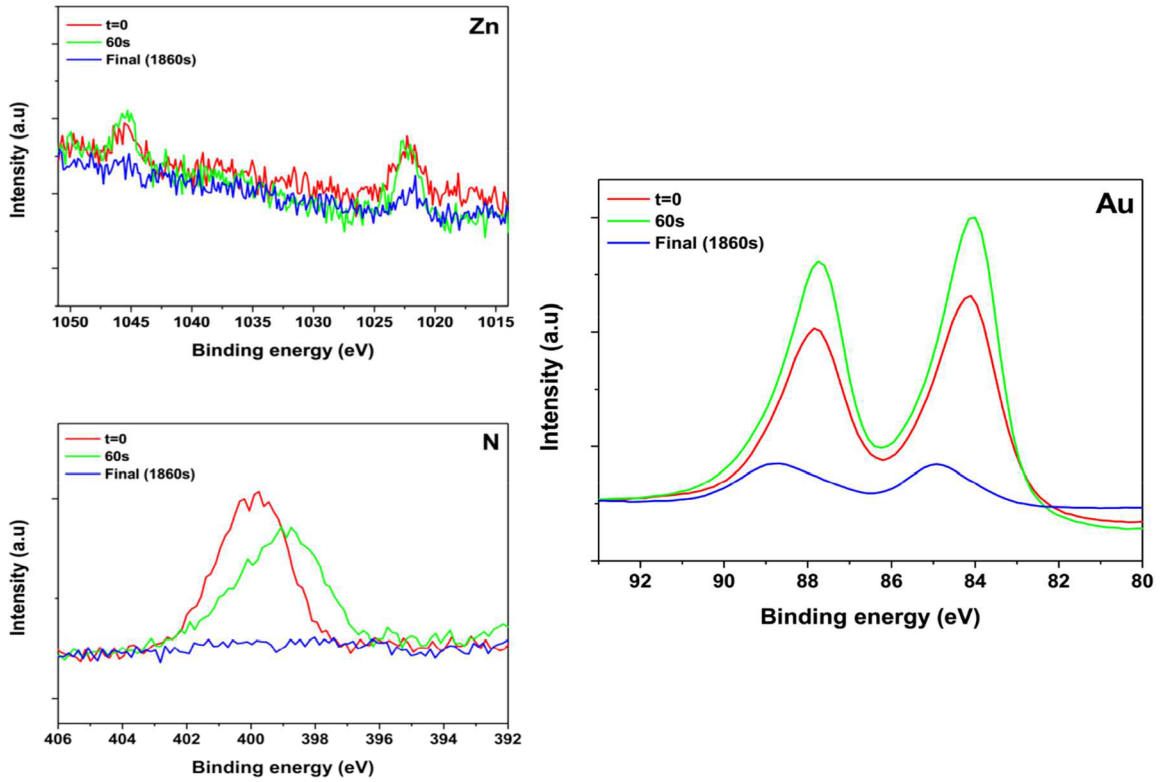

Figure 6. Zn, N, and Au XPS signals at different sputtering times (film depths) for Au-NPT@*5x*-ZIF-8+PSS film.

position is compatible with a BCC structure. This cubic cell has an edge of 12.1 Å, close matching the cubic structure adopted by ZIF-8 MOF. The other reflectivity curves of PSS-capped and Pt-NPT synthesized on PSS-capped films, also present the same defined peak at 0.52 $Å^{-1}$ but the other peaks are not so easily spotted. This would indicate that addition of PSS to the porous structure somehow disturbs ZIF-8 native structure. The extent of this distortion is more evident after Pt-NPT synthesis.

Reflectivity curves were fitted with the model-free fitting software (StochFit)[40] in order to obtain an estimated electron density depth profile of films through scattering length density (SLD) values. This would result in additional information on the question of whether nanoparticles remain surface confined or homogeneously distributed. SLD profiles obtained are presented in Figure 8 (SLD values are reported relative to the Si substrate, and relative thickness scale across the film, with minimum depth on the substrate surface, and maximum at the top film surface). The increased value of SLD throughout thickness after PSS capping, suggest that polymer is not confined (some film expansion can be ascribed to swelling due increased charge from sulfonate moieties). On the other hand, the observed SLD profile after nanoparticle synthesis (Pt-NPT@*5x*-ZIF-8+PSS) does not show thickness increase, but it

DOI: 10.1021/acs.langmuir.7b03083
Langmuir 2018, 34, 425−431

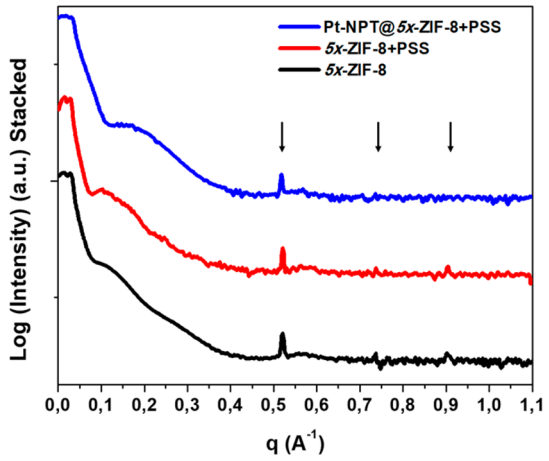

Figure 7. Reflectivity curves of *5x*-ZIF-8, *5x*-ZIF-8+PSS and Pt-NPT@*5x*-ZIF-8+PSS.

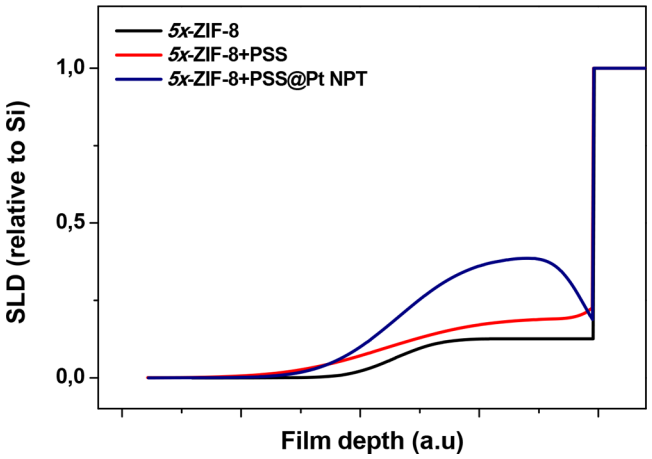

Figure 8. Electron Density Profiles obtained by fitting XRR curves for *5x*-ZIF-8, *5x*-ZIF-8+PSS, and Pt-NPT@*5x*-ZIF-8+PSS films.

does show a dramatic increase in the SLD values also compatible with a nonconfined configuration of high-contrast Pt-NPT. This fact suggests, in line with XPS results above presented for Au, that Pt-NPT does not remain near the film top surface, but rather homogeneously distributed within the PSS-capped mesoporous environment.

CONCLUSIONS

By using a quite straightforward procedure, we have demonstrated that successful modification of surface properties of metal organic frameworks films is possible. Our proof-of-concept makes use of proverbial zeolitic imidazolate framework ZIF-8, a robust and mainly hydrophobic material, and PSS polyelectrolyte, which constitutes an inexpensive and readily available modifying agent. Dip-coating of synthesized films on PSS aqueous solutions, confer an increased polar character to the mesoporous environment, which was demonstrated by performing CV experiments with negatively and positively charged redox probes. It is worth mentioning that noncapped ZIF-8 films present an exclusion effect for negatively charged diffusing-probes caused by both, its hydrophobic character (due to the $-CH_3$ present on 2-methylimidazolate linkers), and a slightly negative Surface Zeta potential. After PSS capping, these two effects can be somehow decoupled, and the increased hydrophilic character of mesoporous channels in the film is evidenced by permeation of both negative and positive molecules.

Taking advantage of the gained insight, we explored the suitability of in situ synthesis to obtain film-embedded metal nanoparticles, via sequential exposure to aqueous solutions of both polar, precursor, and reducing agent (so-called diffusion-reaction approach). For both Pt and Au nanoparticle synthesis using PSS-capped films, nonsegregated NPT distributions were obtained, as revealed by XRR and XPS experiments.

The procedure hereby presented is quite versatile, and with minimum modifications (mainly taking into account affinity between capping agent and selected MOF) could be used as a general strategy toward synthesis of mesoporous films hosting metal nanoparticles, i.e., a composite material with catalytic active centers dispersed within high surface area and chemically versatile scaffolds.

ASSOCIATED CONTENT

Supporting Information

The Supporting Information is available free of charge on the ACS Publications website at DOI: 10.1021/acs.langmuir.7b03083.

Figures S1−S6 (PDF)

AUTHOR INFORMATION

Corresponding Author

*E-mail: mrafti@quimica.unlp.edu.ar (M.R.).

ORCID

Omar Azzaroni: 0000-0002-5098-0612

Matías Rafti: 0000-0003-3393-358X

Notes

The authors declare no competing financial interest.

REFERENCES

(1) Furukawa, H.; Cordova, K. E.; O'Keeffe, M.; Yaghi, O. M. The Chemistry and Applications of Metal-Organic Frameworks. *Science (Washington, DC, U. S.)* **2013**, *341* (6149), 1230444−1230444.

(2) Férey, G. Hybrid Porous Solids: Past, Present, Future. *Chem. Soc. Rev.* **2008**, *37* (1), 191−214.

(3) Ariga, K.; Ji, Q.; Mori, T.; Naito, M.; Yamauchi, Y.; Abe, H.; Hill, J. P. Enzyme Nanoarchitectonics: Organization and Device Application. *Chem. Soc. Rev.* **2013**, *42* (15), 6322.

(4) Vinu, A.; Ji, Q.; Hill, J. P.; Ariga, K. Mesoporous Nanoarchitectonics. In *Manipulation of Nanoscale Materials*; Ariga, K., Ed.; Royal Society of Chemistry: Cambridge, U.K., 2012; Chapter 5, pp 112−128.

(5) Li, P.; Modica, J. A.; Howarth, A. J.; Vargas, L. E.; Moghadam, P. Z.; Snurr, R. Q.; Mrksich, M.; Hupp, J. T.; Farha, O. K. Toward Design Rules for Enzyme Immobilization in Hierarchical Mesoporous Metal-Organic Frameworks. *Chem* **2016**, *1* (1), 154−169.

(6) Liu, W.-L.; Wu, C.-Y.; Chen, C.-Y.; Singco, B.; Lin, C.-H.; Huang, H.-Y. Fast Multipoint Immobilized MOF Bioreactor. *Chem.−Eur. J.* **2014**, *20* (29), 8923−8928.

(7) Cook, T. R.; Zheng, Y. R.; Stang, P. J. Metal-Organic Frameworks and Self-Assembled Supramolecular Coordination Complexes: Comparing and Contrasting the Design, Synthesis, and Functionality of Metal-Organic Materials. *Chem. Rev.* **2013**, *113* (1), 734−777.

(8) Lu, G.; Li, S.; Guo, Z.; Farha, O. K.; Hauser, B. G.; Qi, X.; Wang, Y.; Wang, X.; Han, S.; Liu, X.; et al. Imparting Functionality to a Metal−organic Framework Material by Controlled Nanoparticle Encapsulation. *Nat. Chem.* **2012**, *4* (4), 310−316.

(9) Santos, V. P.; Wezendonk, T. a.; Jaén, J. J. D.; Dugulan, a. I.; Nasalevich, M. a.; Islam, H.-U.; Chojecki, A.; Sartipi, S.; Sun, X.;

DOI: 10.1021/acs.langmuir.7b03083
Langmuir 2018, 34, 425−431

Hakeem, A. a.; et al. Metal Organic Framework-Mediated Synthesis of Highly Active and Stable Fischer−Tropsch Catalysts. *Nat. Commun.* **2015**, *6*, 6451.
(10) Burtch, N. C.; Jasuja, H.; Walton, K. S. Water Stability and Adsorption in Metal−Organic Frameworks. *Chem. Rev.* **2014**, *114* (20), 10575−10612.
(11) Gascon, J.; Corma, A.; Kapteijn, F.; Llabres i Xamena, F. X. Metal Organic Framework Catalysis: Quo Vadis? *ACS Catal.* **2014**, *4* (2), 361−378.
(12) Čejka, J. Metal-Organic Frameworks. Applications from Catalysis to Gas Storage. Edited by David Farrusseng. *Angew. Chem., Int. Ed.* **2012**, *51* (20), 4782−4783.
(13) Bétard, A.; Fischer, R. a. Metal-Organic Framework Thin Films: From Fundamentals to Applications. *Chem. Rev.* **2012**, *112*, 1055−1083.
(14) Liu, B.; Ma, M.; Zacher, D.; Bétard, A.; Yusenko, K.; Metzler-Nolte, N.; Wöll, C.; Fischer, R. a. Chemistry of SURMOFs: Layer-Selective Installation of Functional Groups and Post-Synthetic Covalent Modification Probed by Fluorescence Microscopy. *J. Am. Chem. Soc.* **2011**, *133* (6), 1734−1737.
(15) Tu, M.; Wannapaiboon, S.; Khaletskaya, K.; Fischer, R. a. Engineering Zeolitic-Imidazolate Framework (ZIF) Thin Film Devices for Selective Detection of Volatile Organic Compounds. *Adv. Funct. Mater.* **2015**, *25* (28), 4470−4479.
(16) Zacher, D.; Shekhah, O.; Wöll, C.; Fischer, R. a. Thin Films of Metal−organic Frameworks. *Chem. Soc. Rev.* **2009**, *38* (5), 1418.
(17) Yao, J.; Wang, H. Zeolitic Imidazolate Framework Composite Membranes and Thin Films: Synthesis and Applications. *Chem. Soc. Rev.* **2014**, *43* (13), 4470−4493.
(18) McGuire, C. V.; Forgan, R. S. The Surface Chemistry of Metal−organic Frameworks. *Chem. Commun.* **2015**, *51* (25), 5199−5217.
(19) Horcajada, P.; Serre, C.; Grosso, D.; Boissière, C.; Perruchas, S.; Sanchez, C.; Férey, G. Colloidal Route for Preparing Optical Thin Films of Nanoporous Metal-Organic Frameworks. *Adv. Mater.* **2009**, *21* (19), 1931−1935.
(20) Morozan, A.; Jaouen, F. Metal Organic Frameworks for Electrochemical Applications. *Energy Environ. Sci.* **2012**, *5* (11), 9269.
(21) Ma, W.; Jiang, Q.; Yu, P.; Yang, L.; Mao, L. Zeolitic Imidazolate Framework-Based Electrochemical Biosensor for in Vivo Electrochemical Measurements. *Anal. Chem.* **2013**, *85* (15), 7550−7557.
(22) Yadav, D. K.; Ganesan, V.; Sonkar, P. K.; Gupta, R.; Rastogi, P. K. Electrochemical Investigation of Gold Nanoparticles Incorporated Zinc Based Metal-Organic Framework for Selective Recognition of Nitrite and Nitrobenzene. *Electrochim. Acta* **2016**, *200*, 276−282.
(23) Heinke, L.; Gu, Z.; Wöll, C. The Surface Barrier Phenomenon at the Loading of Metal-Organic Frameworks. *Nat. Commun.* **2014**, *5* (May), 4562.
(24) Brunsen, A.; Calvo, A.; Williams, F. J.; Soler-Illia, G. J. a a; Azzaroni, O. Manipulation of Molecular Transport into Mesoporous Silica Thin Films by the Infiltration of Polyelectrolytes. *Langmuir* **2011**, *27*, 4328−4333.
(25) Calvo, A.; Fuertes, M. C.; Yameen, B.; Williams, F. J.; Azzaroni, O.; Soler-Illia, G. J. a a. Nanochemistry in Confined Environments: Polyelectrolyte Brush-Assisted Synthesis of Gold Nanoparticles inside Ordered Mesoporous Thin Films. *Langmuir* **2010**, *26* (8), 5559−5567.
(26) Rafti, M.; Brunsen, A.; Fuertes, M. C.; Azzaroni, O.; Soler-Illia, G. J. a a. Heterogeneous Catalytic Activity of Platinum Nanoparticles Hosted in Mesoporous Silica Thin Films Modified with Polyelectrolyte Brushes. *ACS Appl. Mater. Interfaces* **2013**, *5* (18), 8833−8840.
(27) Wang, B.; Côté, A. P.; Furukawa, H.; O'Keeffe, M.; Yaghi, O. M. Colossal Cages in Zeolitic Imidazolate Frameworks as Selective Carbon Dioxide Reservoirs. *Nature* **2008**, *453* (7192), 207−211.
(28) Park, K. S.; Ni, Z.; Cote, A. P.; Choi, J. Y.; Huang, R.; Uribe-Romo, F. J.; Chae, H. K.; O'Keeffe, M.; Yaghi, O. M. Exceptional Chemical and Thermal Stability of Zeolitic Imidazolate Frameworks. *Proc. Natl. Acad. Sci. U. S. A.* **2006**, *103* (27), 10186−10191.
(29) Zhong, H.; Wang, J.; Zhang, Y.; Xu, W.; Xing, W.; Xu, D.; Zhang, Y.; Zhang, X. ZIF-8 Derived Graphene-Based Nitrogen-Doped Porous Carbon Sheets as Highly Efficient and Durable Oxygen Reduction Electrocatalysts. *Angew. Chem., Int. Ed.* **2014**, *53* (51), 14235−14239.
(30) Yim, C.; Lee, M.; Kim, W.; Lee, S.; Kim, G.-H.; Kim, K. T.; Jeon, S. Adsorption and Desorption Characteristics of Alcohol Vapors on a Nanoporous ZIF-8 Film Investigated Using Silicon Microcantilevers. *Chem. Commun.* **2015**, *51* (28), 6168−6171.
(31) Chizallet, C.; Lazare, S.; Bazer-Bachi, D.; Bonnier, F.; Lecocq, V.; Soyer, E.; Quoineaud, A. A.; Bats, N. Catalysis of Transesterification by a Nonfunctionalized Metal-Organic Framework: Acido-Basicity at the External Surface of ZIF-8 Probed by FTIR and Ab Initio Calculations. *J. Am. Chem. Soc.* **2010**, *132* (35), 12365−12377.
(32) Lu, G.; Hupp, J. T. Metal−Organic Frameworks as Sensors: A ZIF-8 Based Fabry−Pérot Device as a Selective Sensor for Chemical Vapors and Gases. *J. Am. Chem. Soc.* **2010**, *132* (23), 7832−7833.
(33) Tuninetti, J. S.; Rafti, M.; Azzaroni, O. Early Stages of ZIF-8 Film Growth: The Enhancement Effect of Primers Exposing Sulfonate Groups as Surface-Confined Nucleation Agents. *RSC Adv.* **2015**, *5* (90), 73958−73962.
(34) Zhang, R.; Ji, S.; Wang, N.; Wang, L.; Zhang, G.; Li, J.-R. Coordination-Driven In Situ Self-Assembly Strategy for the Preparation of Metal-Organic Framework Hybrid Membranes. *Angew. Chem., Int. Ed.* **2014**, *53* (37), 9775−9779.
(35) Rafti, M.; Segovia, G. M.; Allegretto, J. A.; Giussi, J. M.; Bindini, E.; Azzaroni, O. Metal − Organic Frameworks Meet Polymer Brushes: Enhanced Crystalline Film Growth Induced by Macromolecular Primers †. *Mater. Chem. Front.* **2017**, *1*, 2256.
(36) Tuninetti, J. S.; Rafti, M.; Andrieu-Brunsen, A.; Azzaroni, O. Molecular Transport Properties of ZIF-8 Thin Films in Aqueous Environments: The Critical Role of Intergrain Mesoporosity as Diffusional Pathway. *Microporous Mesoporous Mater.* **2016**, *220*, 253−257.
(37) Rafti, M.; Marmisollé, W. A.; Azzaroni, O. Metal-Organic Frameworks Help Conducting Polymers Optimize the Efficiency of the Oxygen Reduction Reaction in Neutral Solutions. *Adv. Mater. Interfaces* **2016**, *3* (16), 1600047.
(38) Esken, D.; Turner, S.; Lebedev, O. I.; Van Tendeloo, G.; Fischer, R. a. Au@ZIFs: Stabilization and Encapsulation of Cavity-Size Matching Gold Clusters inside Functionalized Zeolite Imidazolate Frameworks, ZIFs. *Chem. Mater.* **2010**, *22* (10), 6393−6401.
(39) Wei, Y.; Han, S.; Walker, D. A.; Fuller, P. E.; Grzybowski, B. A. Nanoparticle Core/Shell Architectures within MOF Crystals Synthesized by Reaction Diffusion. *Angew. Chem., Int. Ed.* **2012**, *51* (30), 7435−7439.
(40) Danauskas, S. M.; Li, D.; Meron, M.; Lin, B.; Lee, K. Y. C. Stochastic Fitting of Specular X-Ray Reflectivity Data Using StochFit. *J. Appl. Crystallogr.* **2008**, *41*, 1187−1193.

DOI: 10.1021/acs.langmuir.7b03083
Langmuir 2018, 34, 425−431